

Interaction between the Northeastern Boundary of Sgr A East and Giant Molecular Clouds

Sungho Lee¹, Soojong Pak^{1,2*}, Christopher J. Davis³, Robeson M. Herrnstein⁴,
T. R. Geballe⁵, Paul T. P. Ho⁴, and J. Craig Wheeler⁶

¹*Astronomy Program in SEES, Seoul National University, Shillim-Dong, Kwanak-Gu, Seoul 151-742, South Korea*

²*Korea Astronomy Observatory, Whaam-Dong, Youseong-Gu, Taejeon 305-348, South Korea*

³*Joint Astronomy Centre, University Park, 660 North A'ohoku Place, Hilo, HI 96720, USA*

⁴*Harvard-Smithsonian Center for Astrophysics, 60 Garden Street, Cambridge, MA 02138, USA*

⁵*Gemini Observatory, 670 N. A'ohoku Place, Hilo, HI 96720, USA*

⁶*Astronomy Department, University of Texas, Austin, TX 78712, USA*

Accepted 2002 ?? ?. Received 2002 ?? ??; in original form 2002 ?? ??

ABSTRACT

We have detected the $v = 1 \rightarrow 0$ S(1) ($\lambda = 2.1218\mu\text{m}$) and $v = 2 \rightarrow 1$ S(1) ($\lambda = 2.2477\mu\text{m}$) lines of H₂ in the Galactic centre, in a 90×27 arcsec region between the northeastern boundary of the non-thermal source, Sgr A East, and the giant molecular cloud (GMC) M-0.02-0.07. The detected H₂ $v = 1 \rightarrow 0$ S(1) emission has an intensity of $1.6 - 21 \times 10^{-18} \text{ W m}^{-2} \text{ arcsec}^{-2}$ and is present over most of the region. Along with the high intensity, the broad line widths (FWHM = 40 – 70 km s⁻¹) and the H₂ $v = 2 \rightarrow 1$ S(1) to $v = 1 \rightarrow 0$ S(1) line ratios (0.3 – 0.5) can be best explained by a combination of C-type shocks and fluorescence. The detection of shocked H₂ is clear evidence that Sgr A East is driving material into the surrounding adjacent cool molecular gas. The H₂ emission lines have two velocity components at $\sim +50$ km s⁻¹ and ~ 0 km s⁻¹, which are also present in the NH₃(3,3) emission mapped by McGary, Coil, & Ho (2001). This two-velocity structure can be explained if Sgr A East is driving C-type shocks into both the GMC M-0.02-0.07 and the northern ridge of McGary, Coil, & Ho (2001).

Key words: Galaxy: centre – ISM: individual(Sgr A East), molecules – infrared: ISM: lines and bands

1 INTRODUCTION

Sgr A East has frequently been interpreted as a supernova remnant due to its shell structure and non-thermal spectrum (Jones 1974; Goss et al. 1983 and references therein; and see the more recent references in Maeda et al. 2002). Some recent research, however, has suggested that the energetics, size, and elongated morphology (3×4 arcmin or 7×9 pc at $d = 8.5$ kpc) of Sgr A East cannot have been produced by a typical supernova (Yusef-Zadeh & Morris 1987; Mezger et al. 1989). Mezger et al. (1989) estimate the required energy to produce Sgr A East to be more than 4×10^{52} ergs. Modeling of the entire spectrum of Sgr A East by Fatuzzo et al. (1999), which fits very well with the observations of the non-thermal emission of Sgr A East and EGRET γ -ray sources, supports the energy estimate by Mezger et al. (1989). Those authors concluded that a single supernova ex-

plosion could explain the existence of Sgr A East only if it occurred within the cavity formed by the stellar wind from a progenitor star. In that scenario, however, the formation of the cavity takes too much time ($\sim 10^6$ yr) compared with the orbital period ($\sim 10^5$ yr) of matter circling around the Galactic centre (Mezger et al. 1989).

Yusef-Zadeh & Morris (1987) suggested that a different kind of explosive event could create Sgr A East. The energy required to make a huge shell such as Sgr A East has been associated with a ‘hypernova’ (Woosley, Eastman, & Schmidt 1999). Khokhlov & Melia (1996) hypothesize that Sgr A East may be the remnant of a solar mass star tidally disrupted by a massive black hole. Their model can naturally explain the elongated shape of Sgr A East as well as the extreme energetics. However, from their observation with the *Chandra X-ray Observatory*, Maeda et al. (2002) suggest that Sgr A East should be classified as a metal-rich ‘mixed morphology’ supernova remnant. They argue that the model of Khokhlov & Melia (1996) cannot reproduce the

* E-mail: soojong@astro.snu.ac.kr

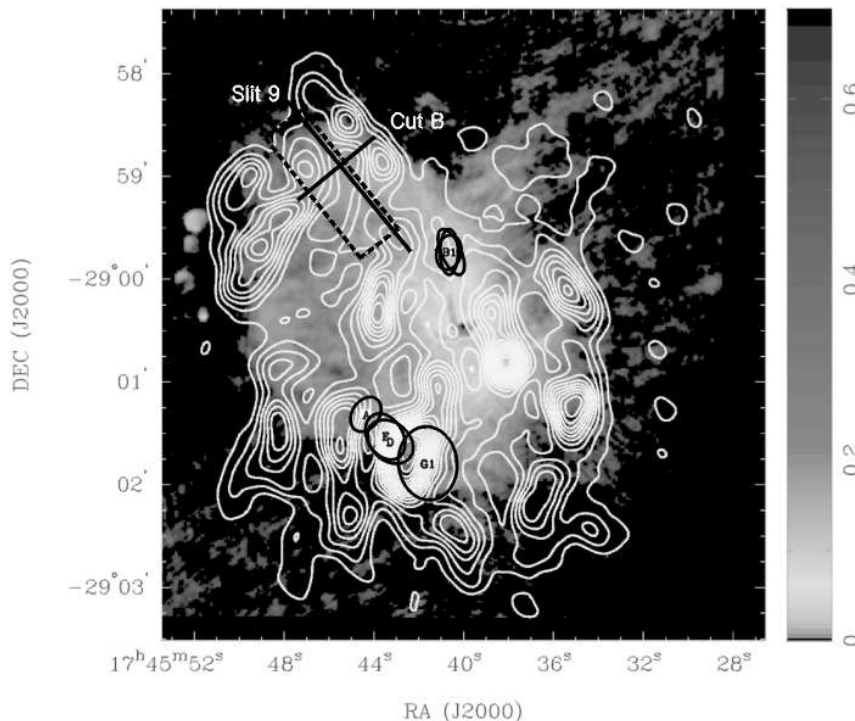


Figure 1. Central 10×15 pc region of the Galaxy. Contours representing the velocity-integrated map of $\text{NH}_3(3,3)$ emission are overlaid on a 6 cm continuum image of Sgr A complex from McGary et al. (2001). The black dot at the centre of image is Sgr A* and the mini spiral is Sgr A West. The CND is traced by the brighter part of continuum surrounding them and Sgr A East is seen by the outer part extended to the boundary of NH_3 contours. The GMC M-0.02-0.07 lies to the east of this region. The dashed box at the northeastern edge of Sgr A East encloses the 90×27 arcsec region observed in H_2 . The two solid lines in the box are the locations from which the H_2 spectra shown in this paper were extracted. Cut B is made across the 10 slits while the NE–SW cut, perpendicular to the edge of Sgr A East, is Slit 9. Letters mark the positions of OH(1720 MHz) masers with error ellipses scaled up by a factor of 15 (Yusef-Zadeh et al. 1999a).

metal-rich abundances observed at the centre of Sgr A East. They also conclude that a single Type II supernova explosion with an energy of 10^{51} ergs into an homogeneous ambient medium with a density of 10^3 cm^{-3} can most simply explain the results of both radio and X-ray observations, and thus that the extreme energy of $\sim 10^{52}$ ergs is not required.

In principle, the energy of the explosive event can be directly measured by studying regions where Sgr A East is colliding with ambient interstellar material. By tracing the dynamics of molecular gas, an interaction between the eastern part of Sgr A East and the giant molecular cloud (GMC) M-0.02-0.07 (also known as the ‘ 50 km s^{-1} cloud’) has been inferred (Genzel et al. 1990; Ho et al. 1991; Serabyn, Lacy, & Achtermann 1992; Mezger, Duschl, & Zylka 1996; Novak 1999; Coil & Ho 2000). Recent observations of $\text{NH}_3(3,3)$ emission in the region show that Sgr A East impacts material to the north and west as well (see Fig. 1) (McGary, Coil, & Ho 2001). As direct evidence of this interaction, several 1720 MHz OH masers, which are a good diagnostic of the continuous, or C-type, shock excitation (Frail et al. 1996; Wardle, Yusef-Zadeh, & Geballe 1999), have been detected along the southern edge of Sgr A East and to the north of the circum-nuclear disc (CND) (Yusef-Zadeh et al. 1996).

Wardle et al. (1999) and Yusef-Zadeh et al. (1999b, 2001) detected H_2 line emission in regions where OH-masers have been detected. In most cases H_2 line emission

arises either from thermal excitation (e.g. by shock heating) or from non-thermal excitation by far-UV absorption (Black & van Dishoeck 1987; Burton 1992; Pak et al. 1998). One can in principle distinguish between these two mechanisms by comparing near-infrared (near-IR) line intensities. The $\text{H}_2 v = 2 \rightarrow 1 \text{ S}(1) / v = 1 \rightarrow 0 \text{ S}(1)$ ratio has been an effective discriminant in a number of shocked regions (where the ratio should be ≤ 0.3) and photodissociation regions (PDRs) (where it is about 0.5 – 0.6). However, a ‘thermal’ line ratio can be observed in a PDR – even though fluorescence is the dominant excitation mechanism – if the gas density is high ($\geq 10^5 \text{ cm}^{-3}$; Sternberg & Dalgarno 1989). Gatley et al. (1984) observed the CND and concluded that the H_2 molecules are excited by collisions, while the results for larger regions (about $2 \times 2 \text{ deg}^2$) by Pak, Jaffe, & Keller (1996a,b) are consistent with non-thermal excitation. The interpretation of Wardle et al. (1999) and Yusef-Zadeh et al. (1999b, 2001) that the line emission in Sgr A East is thermal is supported by the presence of the 1720 MHz OH masers. It is therefore likely that Sgr A East is indeed driving shocks into the adjacent GMCs to the south and into the CND.

The fields observed by Wardle et al. (1999) and Yusef-Zadeh et al. (1999b, 2001) are restricted to the vicinity of the CND and cover only some of the regions where interaction of the Sgr A East shell with surrounding material is expected. Before one can hope to estimate the energy released in the event that created Sgr A East, it is

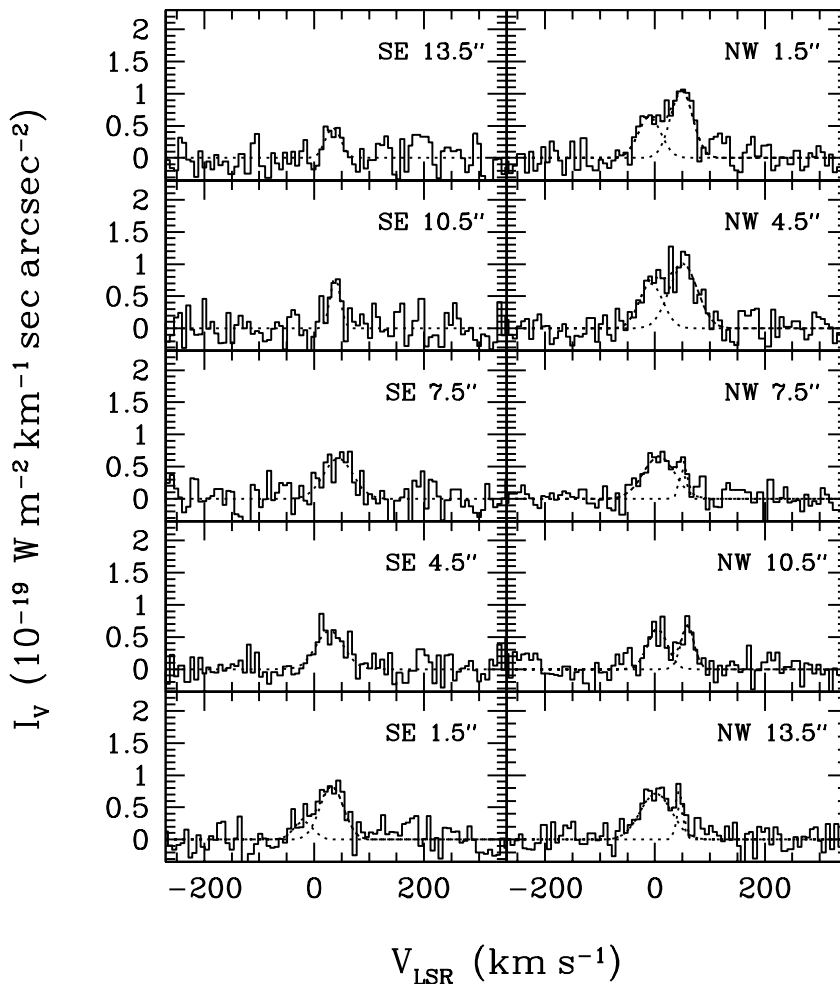


Figure 2. H_2 $v = 1 \rightarrow 0$ S(1) spectra at 10 positions along Cut B. Indicated positions are relative to the centre of the cut ($\alpha = 17^{\text{h}}45^{\text{m}}46^{\text{s}}.1$, $\delta = -28^{\circ}59'01''$; J2000). The dotted lines are Gaussian fits to the observed line profiles. The spectra are not corrected for instrumental broadening.

necessary to observe additional interaction regions in diagnostic lines of H_2 at high spectral resolution. In this paper we present velocity-resolved, near-IR H_2 observations at the northeastern boundary of Sgr A East. By measuring H_2 $v = 2 \rightarrow 1$ S(1) / $v = 1 \rightarrow 0$ S(1) line ratios and line profiles simultaneously we aim to study the excitation and kinematics of the interaction between Sgr A East and M-0.02-0.07.

2 OBSERVATION AND DATA REDUCTION

We observed the H_2 $v = 1 \rightarrow 0$ S(1) ($\lambda = 2.1218\mu\text{m}$) and the H_2 $v = 2 \rightarrow 1$ S(1) ($\lambda = 2.2477\mu\text{m}$) spectra at the 3.8 m United Kingdom Infra-Red Telescope (UKIRT) in Hawaii on 2001 August 3 and 4 (UT), using the Cooled Grating Spectrometer 4 (CGS4; Mountain et al. 1990) with a 31 l/mm echelle grating, 300 mm focal length camera optics and a two-pixel-wide slit. The spatial resolution along the slit was 0.90 arcsec for H_2 $v = 1 \rightarrow 0$ S(1) with the grating angle of $64^{\circ}.691$ and 0.84 arcsec for H_2 $v = 2 \rightarrow 1$ S(1) with $62^{\circ}.127$, respectively; the slit widths on the sky were 0.83

and 0.89 arcsec, respectively, for these two configurations. The slit length is ~ 90 arcsec. The instrumental resolutions, measured from Gaussian fits to sky lines in our raw data, were ~ 17 km s^{-1} for H_2 $v = 1 \rightarrow 0$ S(1) and ~ 19 km s^{-1} for H_2 $v = 2 \rightarrow 1$ S(1), respectively.

Ten parallel slit positions were observed, sampling a 90×27 arcsec area on the northeastern boundary of Sgr A East. The slit was oriented 40° east of north for each measurement; adjacent slit positions were separated by 3 arcsec perpendicular to the slit axis. The coordinates at the centre of the observed area are $\alpha = 17^{\text{h}}45^{\text{m}}45^{\text{s}}.9$, $\delta = -28^{\circ}59'05''$ (J2000) (see Fig. 1). The southwestern part of this region includes the ‘outer H_2 clumps’ from which H_2 emission was detected by Yusef-Zadeh et al. (2001). Only the ninth slit position, hereafter called ‘Slit 9’, was observed in both H_2 $v = 1 \rightarrow 0$ S(1) and H_2 $v = 2 \rightarrow 1$ S(1). The telescope was nodded between object and blank sky positions every 25 minutes, to subtract the background and telluric OH line emission. The sky positions were offset by about $2''.5$ ($\Delta\alpha = -2''.03$, $\Delta\delta = 0''.85$) from the on-source positions.

Initial data reduction steps, involving bias-subtraction and flat-fielding (using an internal blackbody lamp), were

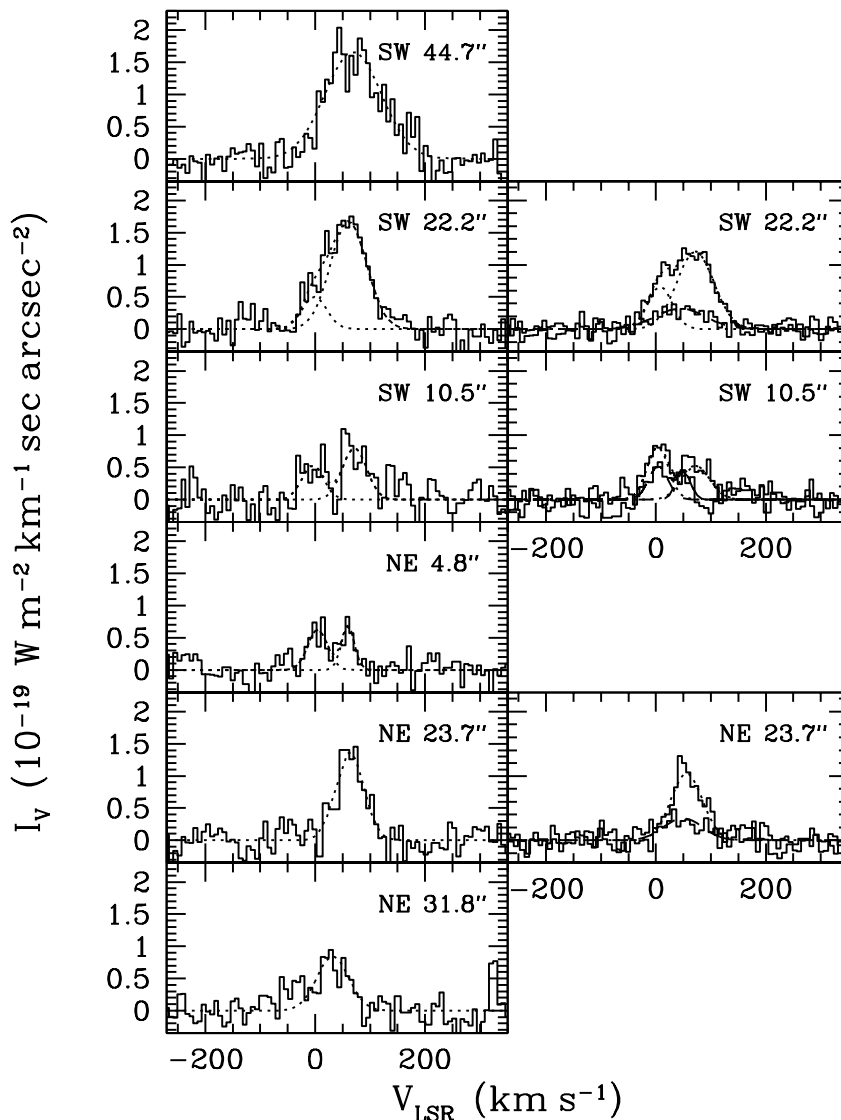


Figure 3. H_2 $v = 1 \rightarrow 0$ S(1) and H_2 $v = 2 \rightarrow 1$ S(1) spectra from six positions along Slit 9. Indicated positions are relative to $\alpha = 17^{\text{h}}45^{\text{m}}45^{\text{s}}.3$, $\delta = -28^{\circ}58'58''$; J2000. Left panels show the H_2 $v = 1 \rightarrow 0$ S(1) spectra. The right three panels present both the H_2 $v = 1 \rightarrow 0$ S(1) and H_2 $v = 2 \rightarrow 1$ S(1) spectra from the positions where H_2 $v = 2 \rightarrow 1$ S(1) emission is detected; these are averaged over 3.4 arcsec on the sky to improve the S/N ratios. The other aspects are the same as Figure 2.

accomplished by the automated Observatory Reduction and Acquisition Control (ORAC) pipeline at UKIRT. IRAF was used for the remainder of the reduction. We corrected the spectral distortion along the dispersion axis using the spectrum of the standard star HR 6496 as a template. The sky OH lines were then used to correct for spatial distortion perpendicular to this axis and also for wavelength calibration. We also corrected for the motions of the Earth and Sun in order to determine local standard of rest (LSR) velocities.

Only part of the flux from a standard star is detected due to the narrow slit; hence for proper flux calibration the measured signal must be corrected. We assumed a circularly symmetric PSF for the star, based on the flux profile along the slit length, to estimate the missing flux. The correction factor, which varies with the seeing, ranged from 2.06 to 2.56. Near-IR emission from the Galactic centre is atten-

uated by interstellar material in the foreground (mostly 4 – 8 kpc from the Galactic centre) and by material in the Galactic centre itself. Since we believe that the H_2 line emission originates from the surface of the cloud, we ignore the latter (Pak et al. 1996a,b) and correct only for foreground extinction; which we assume to be $A_K = 2.5$ mag (Catchpole, Whitlock, & Glass 1990).

3 RESULTS AND DISCUSSION

3.1 H_2 $v = 1 \rightarrow 0$ S(1) emission

Bright ($1.6 - 21 \times 10^{-18} \text{ W m}^{-2} \text{ arcsec}^{-2}$) H_2 emission was detected from most of the observed region (90×27 arcsec) along the northeastern boundary of Sgr A East. We created a SE–NW cut parallel to the boundary of Sgr A East (‘Cut

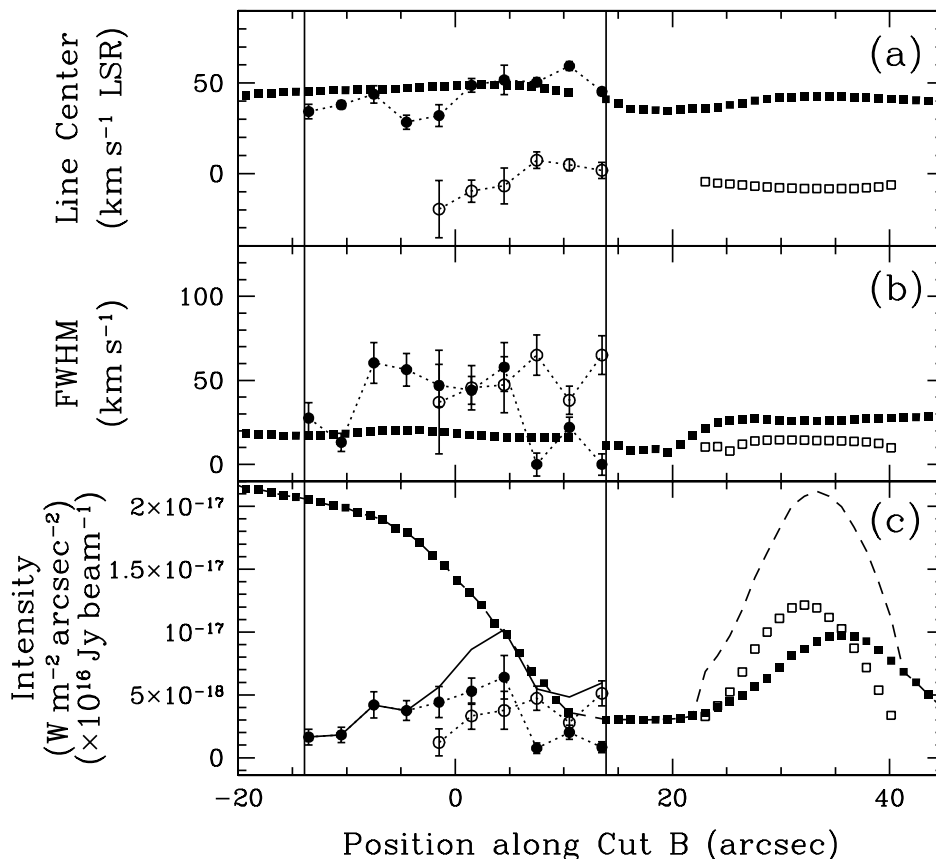


Figure 4. Derived line parameters for the spectra along Cut B: (a) line center velocity; (b) line width; and (c) integrated line intensity. Indicated positions are as in Fig. 2; positive towards NW. The filled circles and the open circles represent the $+50 \text{ km s}^{-1}$ component and the 0 km s^{-1} component of $\text{H}_2 \text{ v} = 1 \rightarrow 0 \text{ S}(1)$ spectra, respectively, and the filled and open squares (the $+50 \text{ km s}^{-1}$ and 0 km s^{-1} component) of the $\text{NH}_3(3,3)$, from McGary et al. (2001). In the panel (c), the solid and dashed lines denote the total intensity of $\text{H}_2 \text{ v} = 1 \rightarrow 0 \text{ S}(1)$ and $\text{NH}_3(3,3)$, respectively, the latter scaled by 10^{-16} . The range of our H_2 observation is denoted by two vertical lines.

B') by extracting spectra from each of the ten slit positions. A second cut perpendicular to the boundary (i.e., SW–NE) is composed of six positions from Slit 9. The positions of Cut B and Slit 9 are marked in Fig. 1. Along Cut B, the intensity of NH_3 emission varies dramatically; we can investigate both high and low density regions along this cut. Slit 9 is the only slit observed both in $\text{H}_2 \text{ v} = 1 \rightarrow 0 \text{ S}(1)$ and $\text{v} = 2 \rightarrow 1 \text{ S}(1)$, the line ratio of which we can use to constrain models for the excitation of H_2 . In this paper, we present the results of these two cuts, rather than the whole data set, as a preliminary report. We aim to concentrate on the excitation mechanism of the detected H_2 emission, and the map the structure and kinematics perpendicular to and parallel to the boundary. From the sixteen $\text{H}_2 \text{ v} = 1 \rightarrow 0 \text{ S}(1)$ spectra in Figs. 2 & 3 we measure line centres and line widths along the interaction region. Each spectrum is well fitted by one or two Gaussian components.

Figs. 4 & 5 show the distributions of the derived $\text{H}_2 \text{ v} = 1 \rightarrow 0 \text{ S}(1)$ line parameters along Cut B and Slit 9, respectively. For direct comparison, we include in these figures data from the $\text{NH}_3(3,3)$ observations of McGary et al. (2001); the NH_3 emission essentially traces the cool ($\lesssim 100 \text{ K}$), dense (10^5 cm^{-3}), cloud material. From these data we note the following.

- In Figs. 4(a) & 5(a) there are two velocity components, at $V_{\text{LSR}} \sim 0 \text{ km s}^{-1}$ and $\sim +50 \text{ km s}^{-1}$. Both components are evident in H_2 and NH_3 , although the 0 km s^{-1} features are not spatially coincident. The variation in the velocity of either component is less than $\sim 20 \text{ km s}^{-1}$ along both Slit 9 and Cut B.
- The H_2 line widths in Figs. 4(b) & 5(b) are much broader than the NH_3 widths and show no obvious trend along either Slit 9 or Cut B.
- Along Cut B, the distribution of the total intensity of H_2 (the solid line in Fig. 4(c)) is quite different from the NH_3 (the dashed line; the units are arbitrarily scaled). The NH_3 emission increases to the southeast as the cut passes deeper into the body of the GMC M-0.02-0.07, but the H_2 emission decreases in this direction. The decrease in H_2 may be explained either by exhaustion of the source of excitation (e.g. shock energy or UV photons) or by obscuration, at the inner, more dense, regions of the cloud, or by the geometry of the interaction region (see Section 3.3).
- Along Slit 9, the distribution of the H_2 intensity (solid line) in Fig. 5(c) is generally similar to that of NH_3 (dashed line). It should be noted that NH_3 is attenuated at positions greater than $+30''$ by the edge of the primary beam in the VLA mosaic (McGary et al. 2001). There is a small discrep-

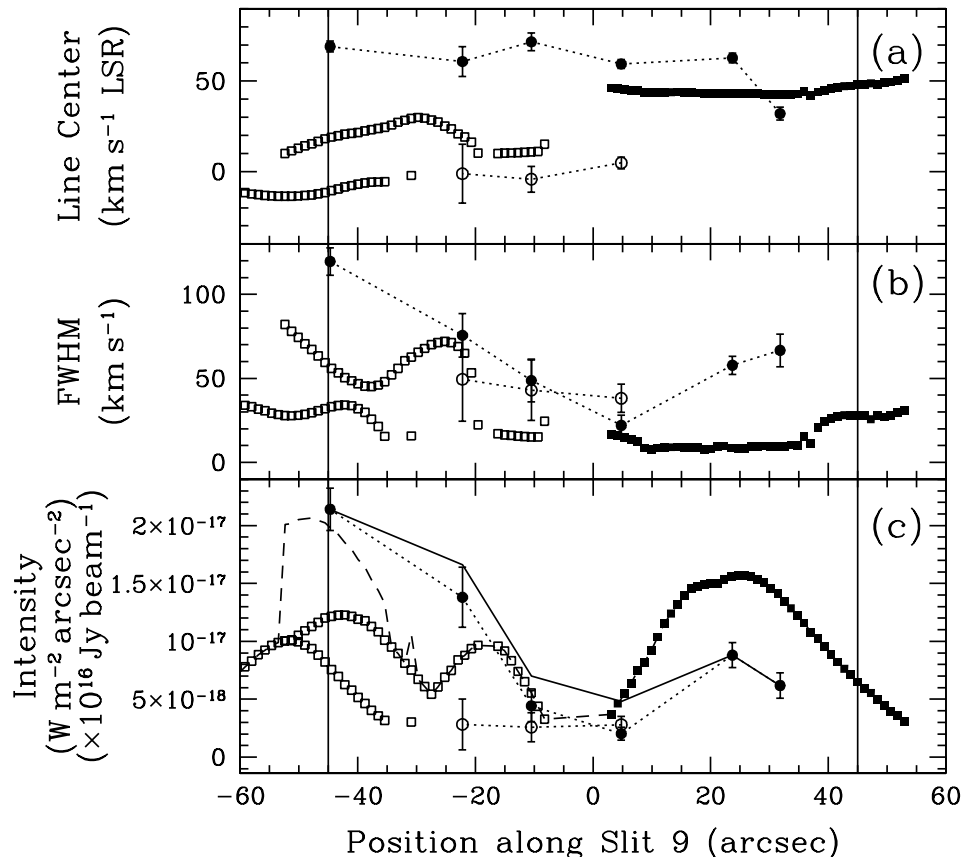


Figure 5. Derived line parameters for the spectra along Slit 9. Indicated positions are as in Fig. 3; positive towards NE. Identities of plotted quantities are as in Fig. 4. The decrease in NH_3 flux at positions greater than $+30''$ is a result of reduced sensitivity at the edge of the mosaic (McGary et al. 2001).

ancy between NH_3 and H_2 between $+10''$ and $+30''$ which may be the result of the same effects discussed in Cut B. Note that Slit 9 covers a very large spatial scale (90 arcsec). The brightest emission along Slit 9, between offsets $-20''$ to $-45''$ (the southwestern part), arises from the outer H_2 clumps of Yusef-Zadeh et al. (2001).

3.2 H_2 excitation

The $\text{H}_2 v = 2 \rightarrow 1 \text{ S}(1)$ line was detected at three locations along Slit 9, at positions NE $23''.7$, SW $10''.5$, and SW $22''.2$ relative to the centre of the slit ($\alpha = 17^{\text{h}}45^{\text{m}}45^{\text{s}}.3$, $\delta = -28^{\circ}58'58''$; J2000). From these data we measured line ratios ($\text{H}_2 v = 2 \rightarrow 1 \text{ S}(1) / v = 1 \rightarrow 0 \text{ S}(1)$) of 0.40 ± 0.12 , 0.51 ± 0.17 , and 0.27 ± 0.07 , respectively (see Fig. 3). At other positions only the $\text{H}_2 v = 1 \rightarrow 0 \text{ S}(1)$ line was detected, with 3σ upper limits to the ratio of 0.5, 0.6, and 0.1 at offsets of NE $31''.8$, NE $4''.8$, and SW $44''.7$ along Slit 9, respectively.

Fluorescent excitation in a low-density PDR ($n(\text{H}_2) < 5 \times 10^4 \text{ cm}^{-3}$) should yield a ratio of about 0.6. A lower ratio is expected in a more dense PDR environment (Black & van Dishoeck 1987), or in a shock. There are two basic types of shock; ‘jump’ or J-type and ‘continuous’ or C-type (see Draine & McKee 1993 for a review). A J-type shock is formed in a highly ionized or weakly magnetized gas. Fluid parameters such as density and temperature un-

dergo a discontinuous change (jump) at the shock front where the molecules may be dissociated. J-type shocks (with velocities greater than about 24 km s^{-1}) will completely dissociate the molecules (Kwan 1977); H_2 emission occurs from a warm, recombination plateau in the post-shock region. J-type shocks typically produce low line intensities and $\text{H}_2 v = 2 \rightarrow 1 \text{ S}(1) / v = 1 \rightarrow 0 \text{ S}(1)$ line ratios as large as 0.5 are possible (Hollenbach & McKee 1989). At lower shock velocities, below the H_2 dissociation speed limit, J-type shocks may yield much lower line ratios; < 0.3 (Smith 1995). In a C-type shock, where the magnetic field softens the shock front via ion-magnetosonic wave propagation so that the fluid parameters change continuously across the shock front, the H_2 dissociation speed limit is much higher ($\sim 45 \text{ km s}^{-1}$; depending on the density and magnetic field strength in the pre-shock gas). Smaller line ratios of about 0.2 are then predicted (Smith 1995; Kaufman & Neufeld 1996).

From the observed ratios alone we are not able to unambiguously distinguish between excitation mechanisms. Our results can either be explained by fast J-type shocks or dense PDRs, or by a combination of fluorescence and either C-type shocks or slow J-type shocks, since the higher line ratios associated with fluorescence will be tempered by the low $\text{H}_2 v = 2 \rightarrow 1 \text{ S}(1)$ intensities associated with collisional excitation in shocks.

To help distinguish between the H_2 excitation mechanisms, we consider kinematic information and the spatial

variation of the line ratio along slit 9. At most positions in Figs. 4(b) & 5(b), the H_2 line widths are high (typically $40 - 70 \text{ km s}^{-1}$, but as high as 120 km s^{-1} in some positions). This suggests shock excitation and turbulent motions in the gas and tends to exclude the pure fluorescence models (in which the H_2 line emission generally arises from the stationary gas at the edges of neutral clouds illuminated by Far-UV photons from early-type stars). However, in other shocked regions the line ratio is found to be constant over a wide range of $H_2 \text{ } v = 1 \rightarrow 0 \text{ S}(1)$ intensities and spatial positions (Davis & Smith 1995; Richter, Graham, & Wright 1995), although this is not necessarily predicted from theory (Draine & McKee 1993). Conversely, in a PDR the ratio is sensitive to the incident FUV flux and the molecular gas density (the $H_2 \text{ } v = 1 \rightarrow 0 \text{ S}(1)$ intensity increases but the $H_2 \text{ } v = 2 \rightarrow 1 \text{ S}(1) / v = 1 \rightarrow 0 \text{ S}(1)$ ratio decreases with increasing gas density or UV intensity; Usuda et al. 1996; Takami et al. 2000). Thus an unchanging $H_2 \text{ } v = 2 \rightarrow 1 \text{ S}(1) / v = 1 \rightarrow 0 \text{ S}(1)$ ratio is found in shocks, while a varying ratio is expected in the pure fluorescent case. The measured line ratio and the $H_2 \text{ } v = 1 \rightarrow 0 \text{ S}(1)$ intensity in Fig. 5(c), show evidence of an anti-correlation in our data, as expected in dense PDRs. Although the wide line profiles point to shock excitation, fluorescence appears to play a significant role at at least some locations.

Considering the kinematics further, we note that J-type shocks produce narrow lines that peak at the velocity of the shock, while C-type shocks produce broader lines which peak at the velocity of the pre-shock gas and extend up to the shock velocity. Figs. 4(a) & 5(a) show that there are two velocity components that are similar in H_2 and NH_3 . The H_2 emission traces hot ($\sim 2000 \text{ K}$) gas and the NH_3 cool ($\lesssim 100 \text{ K}$) gas. Thus, if we assume that shocks are driven by Sgr A East into cold molecular gas, whose velocities are given by the NH_3 data, then fast J-type shocks are inconsistent with our results, due to the low peak velocities of the H_2 lines relative to the molecular clouds.

In summary, then, the wide line profiles and low peak velocities indicate C-type shock excitation. However, the high values of the line ratio at some positions along Slit 9 and the spatial variation in that ratio, point to a fluorescent component to the excitation in some locations. A combination of C-type shocks and fluorescence (see e.g. Fernandes, Brand, & Burton 1997) is therefore the most reasonable explanation for the H_2 excitation. For the fluorescence, the source of the UV radiation could be either nearby early type stars or J-type shocks. However, as noted above, we see no evidence of J-type shocks in our data. Also, we cannot establish whether nearby stars are the source of the UV flux due to the lack of information on where or how many early type stars there are in the region.

3.3 Structure of the interaction region

The extended $+50 \text{ km s}^{-1}$ component of the NH_3 emission traces the GMC M-0.02-0.07, while the 0 km s^{-1} component corresponds to the ‘northern ridge’ of McGary et al. (2001) (see the $NH_3(3,3)$ channel maps in their Fig. 4). The NH_3 component at $\sim +20 \text{ km s}^{-1}$ seen in Fig. 5(a) at negative offsets seems to trace hotter gas according to the $NH_3(2,2)$ to $(1,1)$ line ratio map by McGary et al. (2001), which they suggest may be the result of an impact by Sgr A East.

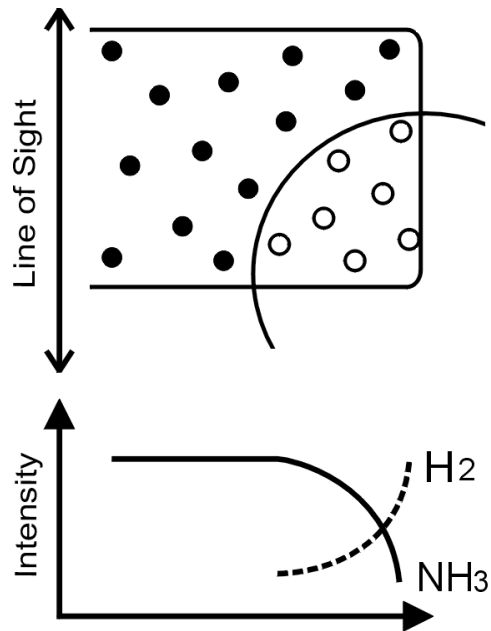


Figure 6. Schematic diagram of Sgr A East and the GMC M-0.02-0.07 along the line of sight. The large partial circle shows the boundary of Sgr A East and the small circles enveloped in a square (M-0.02-0.07) represent the clumpy structure of cloud (see Section 3.3). Open circles are clumps that are being penetrated by shocks, which have destroyed NH_3 but have excited the H_2 into emission. The resulting intensity distribution shows similar trend with the observed results (see the $+50 \text{ km s}^{-1}$ components in Figs. 4(c) & 5(c)).

The difference in line width between NH_3 and H_2 as well as the different spatial locations of their 0 km s^{-1} features (Fig. 5(a)) indicate that the NH_3 and H_2 trace fundamentally different components of the gas. The narrow NH_3 line widths arise in ambient clouds. The broader H_2 line emission traces shocked gas where the NH_3 molecules are likely destroyed. One can envision a situation in which Sgr A East is located adjacent to both M-0.02-0.07 (the $+50 \text{ km s}^{-1}$ component) and the northern ridge (the 0 km s^{-1} component), with Sgr A East driving C-type shocks into these clouds.

On the other hand, the fact that the two H_2 velocity components overlap along the line-of-sight, yet are roughly equally bright seems somewhat unlikely, as one must be attenuated by the molecular cloud associated with the other. The rough equality might be explained by clumpiness of the foreground cloud, regardless of which one is in the foreground, where a small filling factor of high density clumps are embedded within a less dense medium (Burton, Hollenbach, & Tielens 1990). The size of such clumps seems to be $10^{-4} - 10^{-3} \text{ pc}$ (Garay, Moran, & Reid 1987; Churchwell et al. 1987), which is smaller than our resolution of $\sim 1 \text{ arcsec}$ ($\sim 4 \times 10^{-2} \text{ pc}$ at the distance of $\sim 8.5 \text{ kpc}$ to the Galactic center). As illustrated in Fig. 6, this clumpy structure could explain both the observed decrease of NH_3 line emission and the observed increase of H_2 line emission toward the edge of the cloud (see the $+50 \text{ km s}^{-1}$ components in Figs. 4(c) & 5(c)).

4 CONCLUSION

We observed the northeastern part of the Sgr A East shell in order to investigate its interaction with the GMC M-0.02-0.07. The bright H_2 $v = 1 \rightarrow 0$ S(1) emission is strong evidence that Sgr A East is physically adjacent to, and interacting with, M-0.02-0.07.

By comparing the relative intensities of H_2 $v = 1 \rightarrow 0$ S(1) and H_2 $v = 2 \rightarrow 1$ S(1) emission, the distribution of the H_2 $v = 2 \rightarrow 1$ S(1) / $v = 1 \rightarrow 0$ S(1) line ratio, and the radial velocities of the H_2 emission, we can to some extent distinguish between excitation mechanisms for the H_2 . The line ratios tend to support emission in either fast J-type shocks or a dense PDR. However, on considering the bright H_2 $v = 1 \rightarrow 0$ S(1) intensity, the large line widths, and the spatial variation in the line ratio, we conclude that a combination of C-type shocks and fluorescence is required. The presence of shocks is direct evidence that Sgr A East is driving into the surrounding material, and is consistent with the detection of 1720 MHz OH masers to the north of the CND and to the south of Sgr A East (Yusef-Zadeh et al. 1996). Very recently Karlsson et al. (2003) detected the 1720 MHz OH masers also at two positions near our target region, which is more direct evidence supporting our conclusion on the C-type shocks.

The H_2 emission covers most parts of our targeted region (90×27 arcsec). The line profiles are made up of two velocity components both of which extend over a significant portion of the region (15×27 arcsec). We find that the $\text{NH}_3(3,3)$ emission lines observed by McGary et al. (2001) also show a similar kinematic structure, with almost the same velocities. We suggest that the H_2 line emission arises at the interfaces between Sgr A East and two independent molecular clouds, with line-of-sight velocities of $\sim +50$ km s^{-1} (M-0.02-0.07) and ~ 0 km s^{-1} (the northern ridge). Both the observed two velocity components of the H_2 emission and the difference in the intensity distributions between the H_2 and NH_3 emission can be understood if the molecular clouds are composed of small dense clumps with a very small filling factor.

To study the origin and evolution of Sgr A East, it would be important to know the total H_2 luminosity and the total cooling rate (based on that) over the interaction region, which could be compared with those of well studied SNRs. However, it is very difficult to estimate them with the small amount of information we have at present. Given the uncertainty in the emission mechanisms, even estimating the total H_2 luminosity in the small mapped region would be difficult, without considering the entire interaction region. It would be premature for us to estimate the required energy to make the Sgr A East shell. We will be able to do this in the future, after observations of more of the interaction region.

ACKNOWLEDGMENTS

We give special thanks to Young-Sam Yu and Tae-Hyun Kim for their help with the observation. Fig. 1 is reproduced from Fig. 10 of McGary et al. (2001) by permission of the AAS. The United Kingdom Infrared Telescope is operated by the Joint Astronomy Centre on behalf of the U.K.

Particle Physics and Astronomy Council. This work was financially supported by the BK21 Project of the Korean Government. TRG's research is supported by the Gemini Observatory, which is operated by the Association of Universities for Research in Astronomy, Inc., on behalf of the international Gemini partnership of Argentina, Australia, Brazil, Canada, Chile, the United Kingdom and the United States of America.

REFERENCES

- Black J.H., van Dishoeck E.F., 1987, *ApJ*, 322, 412
 Burton M.G., 1992, *Aust. J. Phys.*, 45, 463
 Burton M.G., Hollenbach D.J., Tielens A.G.G.M., 1990, *ApJ*, 365, 620
 Catchpole R.M., Whitelock P.A., Glass I.S., 1990, *MNRAS*, 247, 479
 Coil A.L., Ho P.T.P., 2000, *ApJ*, 533, 245
 Churchwell E., Wood D.O.S., Felli M., Massi M., 1987, *ApJ*, 321, 516
 Davis C.J., Smith M.D., 1995, *ApJ*, 443, L41
 Draine B.T., McKee C.F., 1993, *ARA&A*, 31, 373
 Fatuzzo M., Melia F., Yusef-Zadeh F., Markoff S., 1999, in Falcke H. et al., eds, *ASP Conf. Ser. Vol. 186, The Central Parsecs of the Galaxy*. Astron. Soc. Pac., San Francisco, p. 560
 Fernandes A.J.L., Brand P.W.J.L., Burton M.G., 1997, *MNRAS*, 290, 216
 Frail D.A., Goss W.M., Reynoso E.M., Green A.J., Otrupcek R., 1996, *AJ*, 111, 1651
 Garay G., Moran J.M., Reid M.J., 1987, *ApJ*, 314, 535
 Gatley L., Jones T.J., Hyland A.R., Beattie D.H., Lee T.J., 1984, *MNRAS*, 210, 565
 Genzel R., Stacey G.J., Harris A.I., Geis N., Graf U.U., Poglitsch A., Sutzki J., 1990, *ApJ*, 356, 160
 Goss W.M., Schwarz U.J., Ekers R.D., van Gorkom J.H., 1983, in Danziger J., Gorenstein P., eds, *Proc. IAU Symp. 101, Supernova Remnants and Their X-Ray Emission*. Dordrecht, Reidel, p. 65
 Ho P.T.P., Ho L.C., Szczepanski J.C., Jackson J.M., Armstrong J.T., Barrett A.H., 1991, *Nat*, 350, 309
 Hollenbach D., McKee C.F., 1989, *ApJ*, 342, 306
 Jones T.W., 1974, *A&A*, 30, 37
 Karlsson R., Sjouwerman L.O., Sandqvist Aa., Whiteoak J.B., 2003, submitted to *A&A*
 Kaufman M.J., Neufeld D.A., 1996, *ApJ*, 456, 611
 Khokhlov A., Melia F., 1996, *ApJ*, 457, L61
 Kwan J., 1977, *ApJ*, 216, 713
 Maeda Y. et al., 2002, *ApJ*, 570, 671
 McGary R.S., Coil A.L., Ho P.T.P., 2001, *ApJ*, 559, 326
 Mezger P.G., Duschl W.J., Zylka R., 1996, *ARA&A*, 7, 289
 Mezger P.G., Zylka R., Salter C.J., Wink J.E., Chini R., Kreysa E., Tuffs R., 1989, *A&A*, 209, 337
 Mountain C.M., Robertson D.J., Lee T.J., Wade R., 1990, in Crawford D.L., ed., *Proc. SPIE Vol. 1235, Instrumentation in Astronomy VII*. SPIE, Bellingham, p. 25
 Novak G., 1999, in Falcke H. et al., eds, *ASP Conf. Ser. Vol. 186, The Central Parsecs of the Galaxy*. Astron. Soc. Pac., San Francisco, p. 488
 Pak S., Jaffe D.T., Keller L.D., 1996a, *ApJ*, 457, L43
 Pak S., Jaffe D.T., Keller L.D., 1996b, in Gredel R., ed.,

- ASP Conf. Ser. Vol. 102, The Galactic Center. Astron. Soc. Pac., San Francisco, p. 28
- Pak S., Jaffe D.T., van Dishoeck E.F., Johansson L.E.B., Booth R.S., 1998, *ApJ*, 498, 735
- Richter M.J., Graham J.R., Wright G.S., 1995, *ApJ*, 454, 277
- Serabyn E., Lacy J.H., Achtermann J.M., 1992, *ApJ*, 395, 166
- Smith M.D., 1995, *A&A*, 296, 789
- Sternberg A., Dalgarno A., 1989, *ApJ*, 338, 197
- Takami M., Usuda T., Sugai H., Kawabata H., Suto H., Tanaka M., 2000, *ApJ*, 529, 268
- Usuda T., Sugai H., Kawabata H., Inoue M.Y., Kataza H., Tanaka M., 1996, *ApJ*, 464, 818
- Wardle M., Yusef-Zadeh F., Geballe T.R., 1999, in Falcke H. et al., eds, ASP Conf. Ser. Vol. 186, The Central Parsecs of the Galaxy. Astron. Soc. Pac., San Francisco, p. 432
- Woosley S.E., Eastman R.G., Schmidt B.P., 1999, *ApJ*, 516, 788
- Yusef-Zadeh F., Morris M., 1987, *ApJ*, 320, 545
- Yusef-Zadeh F., Roberts D.A., Goss W.M., Frail D.A., Green A.J., 1996, *ApJ*, 466, L25
- Yusef-Zadeh F., Roberts D.A., Goss W.M., Frail D.A., Green A.J., 1999a, *ApJ*, 512, 230
- Yusef-Zadeh F., Stolovy S.R., Burton M., Wardle M., Ashley M.C.B., 2001, *ApJ*, 560, 749
- Yusef-Zadeh F., Stolovy S.R., Burton M., Wardle M., Melia F., Lazio T.J.W., Kassim N.E., Roberts D.A., 1999b, in Falcke H. et al., eds, ASP Conf. Ser. Vol. 186, The Central Parsecs of the Galaxy. Astron. Soc. Pac., San Francisco, p. 197

This paper has been typeset from a \TeX / \LaTeX file prepared by the author.